Flow–Force Relationships for a Six-State Proton Pump Model: Intrinsic Uncoupling, Kinetic Equivalence of Input and Output Forces, and Domain of Approximate Linearity†

Daniela Pietrobon‡ and S. Roy Caplan*
Department of Membrane Research, The Weizmann Institute of Science, Rehovot 76100, Israel
Received January 4, 1985; Revised Manuscript Received May 10, 1985

ABSTRACT: General flow–force relations have been determined, by the Hill diagram method, for a six-state proton pump model with and without intrinsic uncoupling (molecular slipping). A computer-aided analysis of the resulting sigmoidal flow–force curves has been performed by using a set of physically meaningful rate constants. It is shown that gating effects and apparent irreversibility can arise from sigmoidicity. The regions of approximate linearity in the vicinity of inflection points, which may be far from equilibrium, have been examined with a view to characterization in terms of linear phenomenological equations, with due regard to the problems of kinetic equivalence of the forces and symmetry. The determination of thermodynamic parameters such as the degree of coupling, the phenomenological stoichiometry, and the efficiency in these regions is discussed, and their meaning is analyzed in relation to the parameters characterizing the Onsager domain close to equilibrium. The application of the phenomenological equations of near-equilibrium nonequilibrium thermodynamics to such regions is at best a simplification to be treated with great caution. A knowledge of the distance from equilibrium of the flow-controlling ranges of the forces (i.e., the ranges of approximate linearity) turns out to be crucial for the interpretation of thermodynamic parameters determined by manipulating one of the forces while the other remains constant, as well as for the interpretation of measurements of force ratios at static head. The latter approaches can give good estimates of the magnitude of the mechanistic stoichiometry and of the constant force if the pumps are highly coupled and are operating not far from equilibrium. The force–flow relationships are shown to be modified by intrinsic uncoupling, reflecting the regulatory influence of the forces on the extent and nature of the slip. Thus reaction slip increases, for example, as the force against which the proton pump operates increases. The possible physiological significance of regulated intrinsic uncoupling is discussed.

Coupled processes constitute the basis of biological energy transduction. In the chemiosmotic view (Mitchell, 1966), energy transduction by oxidative phosphorylation in mitochondria and procaryotic bacteria (as well as by photophosphorylation in chloroplasts) is accomplished by two linked proton pumps. Experimental studies of these systems frequently involve stationary-state (or pseudo-stationary-state) measurements on coupled scalar and vector flows, e.g., chemical reactions and transmembrane ionic fluxes, and the corresponding thermodynamic forces: the affinity of the chemical reaction A (the negative Gibbs free energy change) and the electrochemical potential difference of the transported ion, $\Delta\tilde{\mu}$. Linear relations between flows and forces have been found experimentally in many cases in a variety of systems (Padan & Rottenberg, 1973; Lang et al., 1977a,b; Rottenberg & Gutman, 1977; Azzone et al., 1978a; Schwab & Komor, 1977; Dixon & Al-Awqati, 1979; Lanyi & Silverman, 1979; Stucki, 1980b; van Dam et al., 1980; Lemasters & Billica, 1981; Pietrobon et al., 1982; Caplan & Essig, 1983). However, there are also numerous studies in which linearity was not found (Junge, 1970; Gräber & Witt, 1976; Baccarini Melandri et al., 1977; Nicholls & Bernson, 1977; Maloney & Schattschneider, 1980; Gräber, 1982; Hangarter & Good, 1982; Maloney, 1982; van den Berg et al., 1982; Wanders et al., 1982; Zoratti et al., 1982; Clark et al., 1983; McCarthy & Ferguson, 1983). It is therefore important to examine the pattern of flow–force relationships that a representative two-flow coupled process (such as a proton pump model) can generate and, if there are domains of approximate linearity, to analyze their properties. A set of parameters defined by linear (near-equilibrium) nonequilibrium thermodynamics (NET),[1] i.e., the degree of coupling (q), the phenomenological stoichiometry (Z), and the maximum efficiency (η_{max}), can be helpful in the analysis of coupled processes in general or proton pumps in particular (Kedem & Caplan, 1965; Caplan, 1971; Rottenberg, 1979; Stucki, 1980a,b; Pietrobon et al., 1982; Caplan & Essig, 1983). However, the question arises as to whether relationships derived in terms of these parameters for the restricted region of linearity close to equilibrium hold for extended domains of approximate linearity remote from equilibrium.

General current–voltage relations have been derived by Hansen et al. (1981) for a pseudo-two-state model of an ion pump with voltage-independent reaction constants lumped together and by Chapman et al. (1983) for a six-state model of (Na,K)ATPase (see also Läuger, 1979). Similar model studies relating the flows to the chemical potential difference of the transported ion have been described (Gräber & Schlodder, 1981; Tanford, 1982). However, the behavior with respect to the reaction affinity was not studied, and the questions we are concerned with in this paper (intrinsic uncoupling and linearity) were not addressed. The only previous attempts to study domains of linearity (Rottenberg, 1973; van der Meer et al., 1980; Westerhoff, 1983) were restricted to

† This study was supported by two EMBO short-term travel grants enabling D.P. to work in Rehovot.
‡ Permanent address: CNR Unit for the Study of Physiology of Mitochondria, Institute of General Pathology, University of Padua, Padua, Italy.

[1] Abbreviations: MIP, multidimensional inflection point; NET, nonequilibrium thermodynamics; ATPase, adenosinetriphosphatase.

0006-2960/85/0424-5764$01.50/0

single Michaelis–Menten-type reactions. Instead of the proportional flow–force relationship of NET, a simple linear relationship was proposed for the region of approximate linearity around the inflection point of the sigmoidal curve. This type of treatment was then empirically extended to the case of two coupled processes. It is essential to study the legitimacy of this procedure since it is potentially of great value in analyzing experimental data where linearity is found.

In developing their treatment of the linear region discussed above, van Dam et al. (1980) pointed out that if the range of linearity is far from equilibrium, the input and output forces are in general kinetically inequivalent. Hence the system is not symmetrical in the phenomenological sense (Westerhoff, 1983). On the other hand, Caplan, using the Hill diagram method (Hill, 1977), analyzed the flow–force relations for the general case of any number of coupled processes, as well as for the particular case of two coupled processes in a five-state electrogenic pump model (Caplan, 1981), and showed that if coupling is complete the linear region around a multidimensional inflection point (MIP) (Rothschild et al., 1980) is characterized by kinetic equivalence no matter how far it is from equilibrium.

Many workers assume that ion pumps are completely coupled and that all evidence of uncoupling may be attributed to external leaks. However, there is no thermodynamic or kinetic justification for this assumption. Experimental evidence has been put forward indicating that in general ion pumps exhibit a certain degree of intrinsic uncoupling (Eddy, 1980; Pietrobon et al., 1981, 1983; Karlish & Stein, 1982; Frölich et al., 1983; Serpersu & Tsong, 1984; Soumarmon et al., 1984; Westerhoff & Dancsházy, 1984; Zoratti et al., 1984). For example, an occasional pump turnover may occur, hydrolyzing ATP (ATPase pump) or transferring an electron (redox pump), without proton translocation against a gradient (i.e., "reaction slip"). Similarly, occasionally downhill proton translocation may occur without ATP synthesis or reverse electron transport ("proton slip"). It is therefore of interest to investigate the thermodynamic and kinetic properties of intrinsically uncoupled systems. This analysis is greatly facilitated by the diagram method.

We have applied this method to the determination of the general flow–force relations for a six-state proton pump model with and without intrinsic uncoupling. In particular, we examine the properties of the regions of approximate linearity in the vicinity of inflection points which may be far from equilibrium with a view to characterizing them in terms of linear phenomenological equations. The problems of kinetic equivalence of the forces, symmetry, efficiency, and the meaning of the parameters q and Z in these regions will be discussed. It will be shown how the general force–flow relationships are modified by intrinsic uncoupling, reflecting the regulatory influence of the forces on the extent and nature of the slip.

The Model

A proton pump is a macromolecular membrane-bound system that couples an exergonic reaction to an "uphill" flow of protons from one side of the membrane to the other. Any reaction cycle of such a pump must contain the following essential steps: (1) binding of n protons on one side; (2) conformational change that translocates or otherwise changes the accessibility of the bound protons from one side to the other; (3) unbinding of n protons on other side; (4) conformational change that translocates or otherwise changes the accessibility of the empty proton binding site from the second side back to the first; (5) binding of substrate(s) of the driving

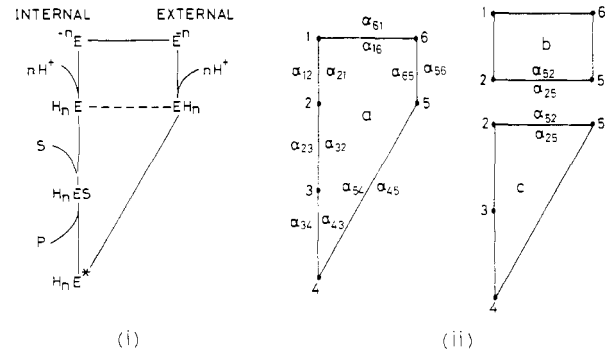

FIGURE 1: Six-state model of a proton pump. (i) Complete diagram. E is a membrane-bound protein with n negatively charged proton binding sites accessible either to the internal medium (states on left side of diagram) or to the external medium (states on right side of diagram). Substrate(s) S and product(s) P are bound or released on the internal side only. The reaction S → P brings about a conformational change in E to E*, in which state it undergoes a transition that changes the accessibility of the bound protons from the internal to the external medium. The transition indicated by a dashed line introduces the possibility of slip (intrinsic uncoupling). (ii) The cycles of the diagram. The states are assigned numbers, and the α_{ij} are first-order or pseudo-first-order rate constants. Cycle a, completely coupled cycle; cycle b, proton slip cycle; cycle c, reaction slip cycle.

reaction; (6) conversion of bound substrate(s) to bound product(s); (7) unbinding of product(s). We will confine ourselves to a minimal model of six steps, assuming that the substrate–product conversion is very fast as is often done in Michaelis–Menten kinetics (Laidler, 1958), and as has been found experimentally for the mitochondrial ATPase (Grubmeyer et al., 1982; O'Neal & Boyer, 1984). Various sequences of the transitions may be chosen: the particular ordered sequence adopted is shown in Figure 1i. For our purposes the order of the sequence of transitions is unimportant—we have chosen the order that allows us to introduce intrinsic uncoupling in the simplest possible way. The possibility of uncoupled cycles is indicated by the dashed transition in Figure 1i. Both completely coupled cycle a and uncoupled cycles b and c are shown in Figure 1ii. The rate constants α_{ij} in Figure 1ii are either first order or pseudo first order: in binding transitions such as the transition 2–3 for substrate binding, $\alpha_{23} = c_S\alpha^*_{23}$, where c_S is the concentration of substrate and α^*_{23} is the second-order rate constant.

In the model considered in Figure 1 the empty proton binding sites are taken to be negatively charged. Consequently, the rate constants of the transitions between the two states 1 and 6 are dependent on the electrical potential gradient. From thermodynamic considerations (Hill, 1977; Caplan, 1981)

$$\alpha_{16}/\alpha_{61} = [\alpha_{16}(0)/\alpha_{61}(0)]e^{-(nF/RT)\Delta\psi_m} \quad (1)$$

where $\Delta\psi_m$ ($=\psi_m^{in} - \psi_m^{ex}$) is the electrical potential difference between the planes in the membrane corresponding to the positions of the n empty binding sites in states 1 and 6 and $\alpha_{16}(0)$ and $\alpha_{61}(0)$ are the values of the rate constants when $\Delta\psi_m = 0$. If these planes coincide with the two surfaces of the membrane, $\Delta\psi_m$ is the electrical potential difference across the membrane, which is related to the bulk-phase potential difference $\Delta\psi$ through the phase-boundary potentials $\Delta\psi_b^{in}$ ($=\psi_m^{in} - \psi^{in}$) and $\Delta\psi_b^{ex}$ ($=\psi_m^{ex} - \psi^{ex}$):

$$\Delta\psi = (\psi^{in} - \psi^{ex}) = \Delta\psi_m + (\Delta\psi_b^{ex} - \Delta\psi_b^{in}) \quad (2)$$

For simplicity, considering a symmetrical Eyring barrier (Geck & Heinz, 1976; Läuger, 1979; Hansen et al., 1981; Chapman et al., 1983), the individual rate constants are given by

$$\alpha_{16} = \alpha_{16}(0)e^{-(nF/2RT)\Delta\psi_m},\ \alpha_{61} = \alpha_{61}(0)e^{(nF/2RT)\Delta\psi_m} \quad (3)$$

In this model the binding of protons in transitions 1–2 and 6–5

is considered to be essentially a diffusion-controlled process. Hence we have assigned the effects of the phase-boundary potentials $\Delta\psi_b^{in}$ and $\Delta\psi_b^{ex}$ entirely to the rates of unbinding, i.e., to the rate constants α_{21} and α_{56}, respectively (Caplan, 1981). The planes corresponding to the positions of the binding sites need not, of course, coincide with the inner and outer membrane surfaces. If not, part of the voltage drop would lie between the surfaces and the binding sites and the binding constants α_{12} and α_{65} would become $\Delta\psi$ dependent. Such cases are not considered here.

If the number of protons translocated per cycle a, n (the mechanistic stoichiometry), is higher than 1, the transitions between states 1 and 2 and states 5 and 6 are actually "reduced" transitions (Hill, 1977) involving a number of partially protonated intervening transient states. The corresponding pseudo-first-order rate constants are hence complex functions of the proton concentrations and the rate constants of the elementary transitions (see Appendix 1). If the reaction gives rise to more than one product (as in the case, for example, of ATP hydrolysis), the transitions between states 3 and 4 are reduced transitions involving one transient intervening state, and the rate constants are functions of those of the elementary transitions and the product concentration (see Appendix 1).

The model presented above may be used as a simplified representation of the ATPase proton pump, where obviously S represents ATP and P corresponds to both ADP and P_i. We shall use the same model, as discussed below, to compare simulated behavior with experimental results related to the coupling between electron transfer from succinate to oxygen and proton transport in mitochondria (Pietrobon et al., 1982). In this case S represents succinate and P corresponds to both fumarate and H^+, and the transitions between states 4 and 5 are reduced as a consequence of intervening transient states involved in the reaction with O_2. This scheme would then correspond to one of the possible ordered sequences of the general random-sequence cube model proposed by Wikström et al. (1981) for a redox pump.

Flow–Force Relationships

The Hill diagram method enables one to write down at sight the kinetic relationships between the flows and the thermodynamic forces for any given cyclic or multicyclic enzymatic reaction scheme. The relevant forces for the model in Figure 1 are $A + n\Delta\tilde{\mu}_H$ ($A = RT \ln (Kc_S/c_P)$, where K is the equilibrium constant, $\Delta\tilde{\mu}_H = \tilde{\mu}_H^{in} - \tilde{\mu}_H^{ex} = RT \ln (c_H^{in}/c_H^{ex}) + F\Delta\psi$ for fully coupled cycle a, $\Delta\tilde{\mu}_H$ for uncoupled cycle b ("proton slip"), and A for uncoupled cycle c ("reaction slip"). If we consider only completely coupled cycle a, the steady-state reaction flow J_r and proton flow J_H are given by

$$J_r = a[e^{(A+n\Delta\tilde{\mu}_H)/RT} - 1] \quad (4)$$

$$a = f_a(c_H^{in}, c_H^{ex}, c_S, c_P, \Delta\psi)$$

$$J_H = nJ_r \quad (5)$$

where a is a function of all the concentrations and the electrical potential difference, as indicated, as well as all the rate constants of the diagram (Hill, 1977; Caplan, 1981). On the other hand, if we consider the entire model including slip cycles b and c, we must add the contributions of these cycles to the steady-state flows, and the equations become

$$J_r = a[e^{(A+n\Delta\tilde{\mu}_H)/RT} - 1] + c[e^{A/RT} - 1] \quad (6)$$

$$c = f_c(c_H^{in}, c_H^{ex}, c_S, c_P, \Delta\psi)$$

$$J_H = na[e^{(A+n\Delta\tilde{\mu}_H)/RT} - 1] + nb[e^{n\Delta\tilde{\mu}_H/RT} - 1] \quad (7)$$

$$b = f_b(c_H^{in}, c_H^{ex}, c_S, c_P, \Delta\psi)$$

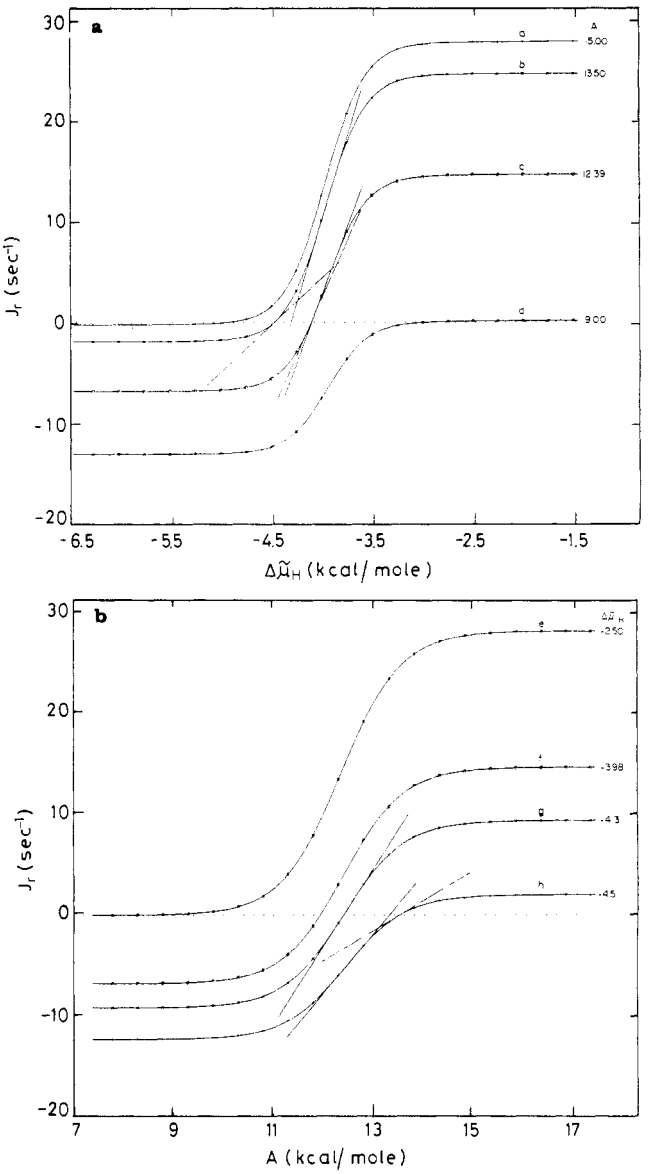

FIGURE 2: Completely coupled pump (pump A). Dependence of J_r on $\Delta\tilde{\mu}_H$ for different constant values of A (a) and of J_r on A for different constant values of $\Delta\tilde{\mu}_H$ (b). The reaction is assumed to be ATP hydrolysis, so that positive values of J_r represent rates of ATP hydrolysis, whereas negative values of J_r represent rates of ATP synthesis. A is varied by varying c_{ATP}, and $\Delta\tilde{\mu}_H$ by varying $\Delta\psi$. The parameters of the simulation are as follows: $n = 3$, $K = 1.71 \times 10^6$ M, $c_{ADP} = 10^{-4}$ M, $c_{P_i} = 10^{-2}$ M, $pH_{in} = pH_{ex} = 7.4$, $\Delta\psi_b^{in} = 0$, $\Delta\psi_b^{ex} = -50$ mV, $\alpha_{12} = 4 \times 10^2$ s^{-1}, $\alpha_{21} = 40$ s^{-1}, $\alpha_{32} = 5 \times 10^3$ s^{-1}, $\alpha_{34} = 10^2$ s^{-1}, $\alpha_{43} = 10^2$ s^{-1}, $\alpha_{45} = 10^2$ s^{-1}, $\alpha_{54} = 10^2$ s^{-1}, $\alpha_{56} = 10^3$ s^{-1}, $\alpha_{65} = 10^3$ s^{-1}, $\alpha_{25} = 5.85 \times 10^{-30}$ s^{-1}, $\alpha_{52} = 1 \times 10^{-20}$ s^{-1}, $\alpha^*_{23} = 5 \times 10^6$ M^{-1} s^{-1}, $\alpha_{16}(0) = 10^2$ s^{-1}, $\alpha_{61}(0) = 4.98 \times 10^7$ s^{-1}.

It is seen that the stoichiometric relationship between J_r and J_H no longer exists. Note that the coefficient a in the latter case contains the rate constants of the slip-generating transition 2–5 (cf. Appendix 2). Figures 2 and 3 show simulations of the flow–force relationships, eq 6 and 7, for the two sets of rate constants. The values of α_{25} and α_{52} have here deliberately been set very small in our general simulation program so that the contributions of uncoupled cycles b and c are negligible, and eq 6 and 7 essentially reduce to the equations for the completely coupled case, eq 4 and 5. In both figures, panel a depicts the variation of J_r with $\Delta\tilde{\mu}_H$ at different constant values of A, while panel b depicts the variation of J_r with A at different constant values of $\Delta\tilde{\mu}_H$. Figure 2 corresponds to the case of a kinetically reversible pump (pump A). The simulations were performed on the basis of the ATPase pump,

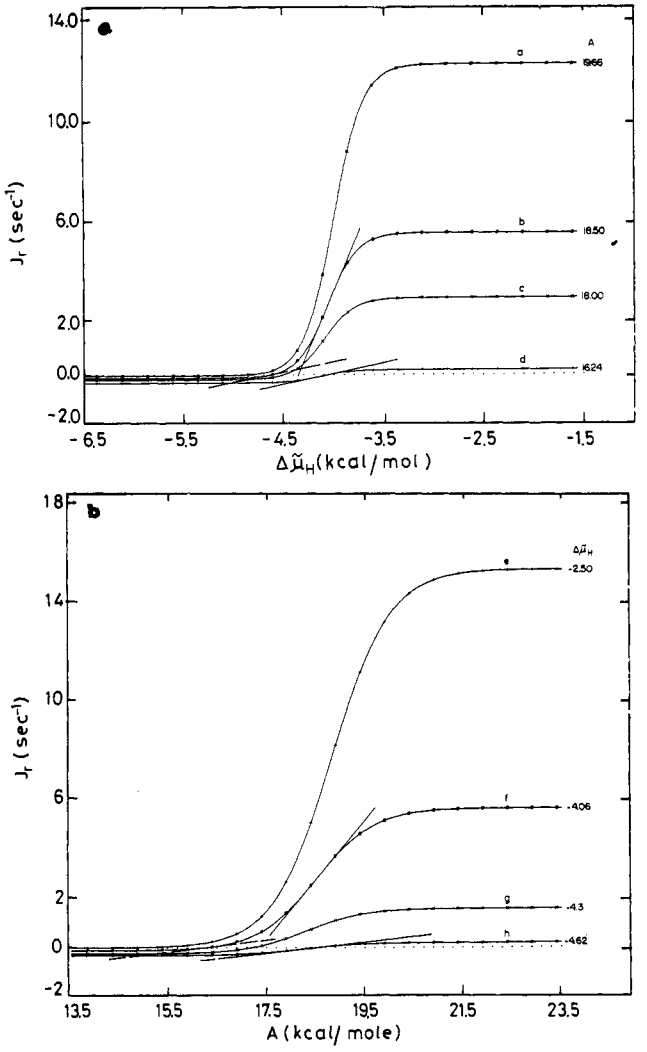

FIGURE 3: Completely coupled pump (pump B). As for Figure 2, but the reaction is assumed to be electron transfer between succinate and oxygen so that J_r represents electron flow. The affinity A corresponds to the transfer of a single electron and is varied by varying $c_{succinate}$. $\Delta\tilde{\mu}_H$ is varied by varying $\Delta\psi$. The parameters of the simulation are as follows: $n = 4$, $K = 1.31 \times 10^{13}$ M (at pH = 7.4 and $P_{O_2} = 0.2$ atm), $c_{fumarate} = 5 \times 10^{-5}$ M, $pH_{in} = pH_{ex} = 7.4$, $\Delta\psi_b^{in} = 0$, $\Delta\psi_b^{ex} = -50$ mV, $\alpha_{12} = 4 \times 10^2$ s^{-1}, $\alpha_{21} = 5$ s^{-1}, $\alpha_{32} = 8 \times 10^4$ s^{-1}, $\alpha_{34} = 4 \times 10^2$ s^{-1}, $\alpha_{43} = 4 \times 10^2$ s^{-1}, $\alpha_{45} = 40$ s^{-1}, $\alpha_{54} = 0.4$ s^{-1}, $\alpha_{56} = 10^2$ s^{-1}, $\alpha_{65} = 10^5$ s^{-1}, $\alpha_{25} = 6.75 \times 10^{-33}$ s^{-1}, $\alpha_{52} = 1 \times 10^{-20}$ s^{-1}, $\alpha^*_{23} = 1 \times 10^6$ M$^{-1/2}$ s^{-1}, $\alpha_{16}(0) = 1.3 \times 10^2$ s^{-1}, $\alpha_{61}(0) = 10^{12}$ s^{-1}.

using the equilibrium constant for hydrolysis of ATP and $n = 3$ H^+/ATP. On the other hand, Figure 3 corresponds to the case of a kinetically irreversible (or practically irreversible) pump (pump B). In this case the equilibrium constant of the electron transfer reaction from succinate to oxygen was used with $n = 4$ H^+/e.

All of the curves shown in Figures 2 and 3 are simple sigmoids exhibiting two regions of saturation and an inflection point around which a region of approximate linearity extends almost over the entire range in which force controls flow. The sets of rate constants, apart from satisfying microscopic reversibility and the constraints due to the reductions of the model, were chosen so as to situate the flow-controlling ranges of forces and the values of the flows close to the experimentally determined ones (Tanford, 1982). From Figures 2a and 3a it can be seen that the total range of control of the flows by $\Delta\tilde{\mu}_H$ is confined within very narrow limits, approximately 1 kcal/mol. The sensitivity of the flows to $\Delta\tilde{\mu}_H$, i.e., the steepness of the curves, is determined, for a given set of rate constants, by n. As n decreases, the slope decreases, and correspondingly

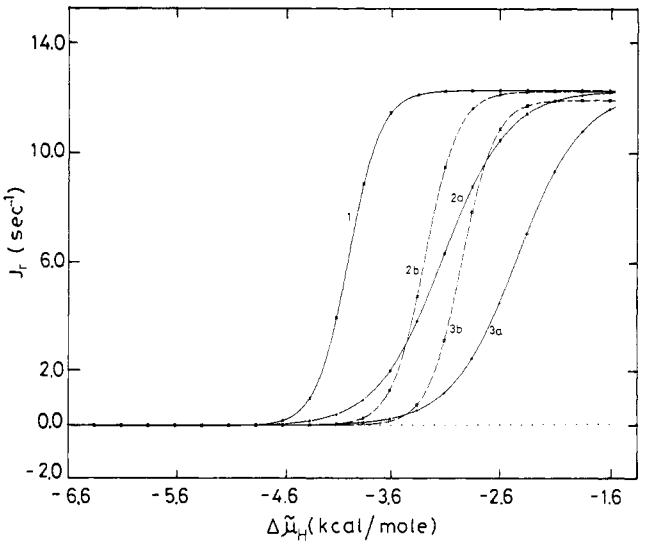

FIGURE 4: Kinetic inequivalence of $\Delta\psi$ and ΔpH. Completely coupled pump B at high affinity ($A = 19.66$ kcal/mol) with rate constants as in Figure 3 except for $\alpha_{16}(0)$ and $\alpha_{61}(0)$, which are as follows: for curve 1, $\alpha_{16}(0) = 1.3 \times 10^2$ s^{-1}, $\alpha_{61}(0) = 10^{12}$ s^{-1}; for curves 2a and 2b, $\alpha_{16}(0) = 1.3 \times 10^{-3}$ s^{-1}, $\alpha_{61}(0) = 10^7$ s^{-1}; for curves 3a and 3b, $\alpha_{16}(0) = 1.3 \times 10^{-4}$ s^{-1}, $\alpha_{61}(0) = 10^6$ s^{-1}. For solid lines (a), $\Delta\tilde{\mu}_H$ was varied by varying $\Delta\psi$ ($pH_{in} = pH_{ex} = 7.4$). For dashed lines (b), $\Delta\tilde{\mu}_H$ was varied by varying c_H^{ex} ($\Delta\psi = -150$ mV, $pH_{in} = 7.4$). In the case of curve 1, the two lines coincide.

the span of the region of approximate linearity increases.

An important consequence of the sigmoidicity of the curves is illustrated in Figure 2. In Figure 2a, curve c (corresponding to $A = 12.39$ kcal/mol) shows the expected behavior for a reversible pump: when $|\Delta\tilde{\mu}_H| > |\Delta\tilde{\mu}_H^{eq}|$ (i.e., the value of $\Delta\tilde{\mu}_H$ at which $J_r = 0$; $|\Delta\tilde{\mu}_H^{eq}| = A/n$), ATP synthesis occurs, while when $|\Delta\tilde{\mu}_H| < |\Delta\tilde{\mu}_H^{eq}|$, hydrolysis occurs. However, for the same pump, curve a (at higher affinity) shows virtually zero synthesis at $|\Delta\tilde{\mu}_H| > |\Delta\tilde{\mu}_H^{eq}|$, while curve d (at low affinity) shows virtually zero hydrolysis at $|\Delta\tilde{\mu}_H| < |\Delta\tilde{\mu}_H^{eq}|$. Note that the same curve, curve d, is obtained for all the range of values of A corresponding to the lower saturated region of the curves in Figure 2b. Hence in this range J_r is virtually zero even under the condition $A/n > |\Delta\tilde{\mu}_H|$, so that equilibrium could only be established after an extremely long time. This behavior might well explain the experimental result that below certain values of $|\Delta\tilde{\mu}_H|$ the ratio between the phosphate potential and $|\Delta\tilde{\mu}_H|$ increased (provided that ATP hydrolysis was needed to reach the true equilibrium state) [see, for example, Azzone et al. (1978b)].

In this study we have varied $\Delta\tilde{\mu}_H$ by varying $\Delta\psi$. However, in general we do not expect kinetic equivalence of $\Delta\psi$ and ΔpH, and hence the flow–force relationships may depend on which of the two parameters is varied. As is seen in Figure 4, this is indeed the case. Kinetic equivalence between the components of $\Delta\tilde{\mu}_H$ is governed by a set of specific conditions limiting the relative magnitudes of the rate constants (Hansen et al., 1981). Without entering into details, we note that these conditions have been satisfied by the set of rate constants that give rise to curve 1 of Figure 4. However, for the two sets of rate constants that give rise to curves 2a,b and 3a,b different behavior is obtained depending on whether $\Delta\psi$ or ΔpH is varied (note the different slopes of the regions of approximate linearity and the shift of the inflection points). Also, we have varied A by varying the substrate concentration, which in general will not be equivalent to varying the product concentration.

Table I: Values of Individual Cycle Fluxes Corresponding to the Flow–Force Relationships Shown in Figure 5 at Low and High $\Delta\tilde{\mu}_H$

q^{ons}	$nJ_a(1)^a$ (s^{-1})	$nJ_a(r)^b$ (s^{-1})	$nJ_b(1)$ (s^{-1})	$nJ_b(r)$ (s^{-1})	$J_c(1)$ (s^{-1})	$J_c(r)$ (s^{-1})
1.00	−0.50	83.57	-0.10×10^{-21}	-0.27×10^{-28}	0.25×10^{-20}	0.28×10^{-20}
0.91	−0.47	82.87	-0.95×10^{-1}	-0.26×10^{-7}	2.30	0.28
0.69	−0.37	80.17	−0.37	-0.13×10^{-6}	8.98	1.34
0.41	−0.20	71.47	−0.82	-0.46×10^{-6}	19.75	4.76
0.15	−0.06	45.27	−1.21	-0.14×10^{-5}	29.06	15.09
0.00	-0.67×10^{-10}	0.99×10^{-7}	−1.37	-0.31×10^{-5}	32.94	32.92

[a] $J_x(l)$ represents the value of J_x in the left-hand saturated region, specifically at $\Delta\tilde{\mu}_H = -6$ kcal/mol. [b] $J_x(r)$ represents the value of J_x in the right-hand saturated region, specifically at $\Delta\tilde{\mu}_H = -1$ kcal/mol.

Characteristics of Intrinsic Uncoupling

In this section we shall analyze the behavior of the pump in terms of its constituent cycles when intrinsic uncoupling is significant. Consider first Figure 5a, which presents a family of curves corresponding to different degrees of coupling showing J_r as a function of $\Delta\tilde{\mu}_H$. The parameter used is the degree of coupling q^{ons} characterizing the linear domain near equilibrium where Onsager symmetry holds. The limiting curve at $q^{ons} = 1$ in Figure 5a is identical with curve a of Figure 2a. This is the ATP-driven pump operating at high affinity in the proton-pumping direction (i.e., $A > 0$, $\Delta\tilde{\mu}_H < 0$). As can be seen, decreasing q^{ons} results in an increase in the hydrolysis rate at all values of $\Delta\tilde{\mu}_H$. The changes in the various curves at different values of q^{ons} as compared with the curve at $q^{ons} = 1$ primarily reflect the contribution of cycle c, the reaction slip (cf. eq 6). It is seen that this contribution increases as $|\Delta\tilde{\mu}_H|$ increases. Evidently, the higher the force against which the pump moves protons, the higher the probability of reaction slip. Inspection of the model (Figure 1) leads to the same conclusion: as $\Delta\psi$ becomes more negative, state 6 becomes more highly populated (cf. eq 3), and consequently state 5 also becomes more populated, leading to an increased transition flux from state 5 to state 2. Thus the probability of cycle c increases at the expense of that of cycle a. In a sense the two cycles may be regarded as in "competition" with each other. Explicit expressions may be written for the individual unidirectional cycle probabilities, which have the form of a cycle rate constant multiplied by the mean time between all cycle completions (Hill, 1977). Since their sum is unity, one probability cannot increase without a concomitant decrease in one or more of the others.

The change in the kinetics of cycle a as a consequence of uncoupling is seen clearly in Figure 5b, where J_H is shown as a function of $\Delta\tilde{\mu}_H$ for the same pump. Here one might have supposed that the differences in the curves as compared with the curve at $q^{ons} = 1$ are due to the contribution of cycle b (cf. eq 7). However, the decrease in J_H seen in Figure 5b as intrinsic uncoupling increases is also found at zero $\Delta\tilde{\mu}_H$, where the contribution of cycle b should be zero. This decrease therefore reflects a decreasing probability of cycle a as a consequence of the competition mentioned above. There appears to be only a very small contribution of cycle b at high $|\Delta\tilde{\mu}_H|$. In this case cycle c is essentially the only cycle operating. The individual values of the cycle fluxes (see Appendix 2) have been checked and support the above conclusions (see Table I).

Figure 6 shows the same pump at low affinity working in the ATP synthesis direction (using the same sign convention as before, so that again $A > 0$, $\Delta\tilde{\mu}_H < 0$). The curve at $q^{ons} = 1$ in Figure 6a corresponds to curve d of Figure 2a. In Figure 6b we see the effect of an increasing contribution of cycle b, i.e., in this case proton slip is occurring. The lowest curve, for which $q^{ons} \approx 0$, gives the relationship between J_H and $\Delta\tilde{\mu}_H$ characteristic of completely uncoupled pumps, which under these conditions act as proton leaks. Note the very steep

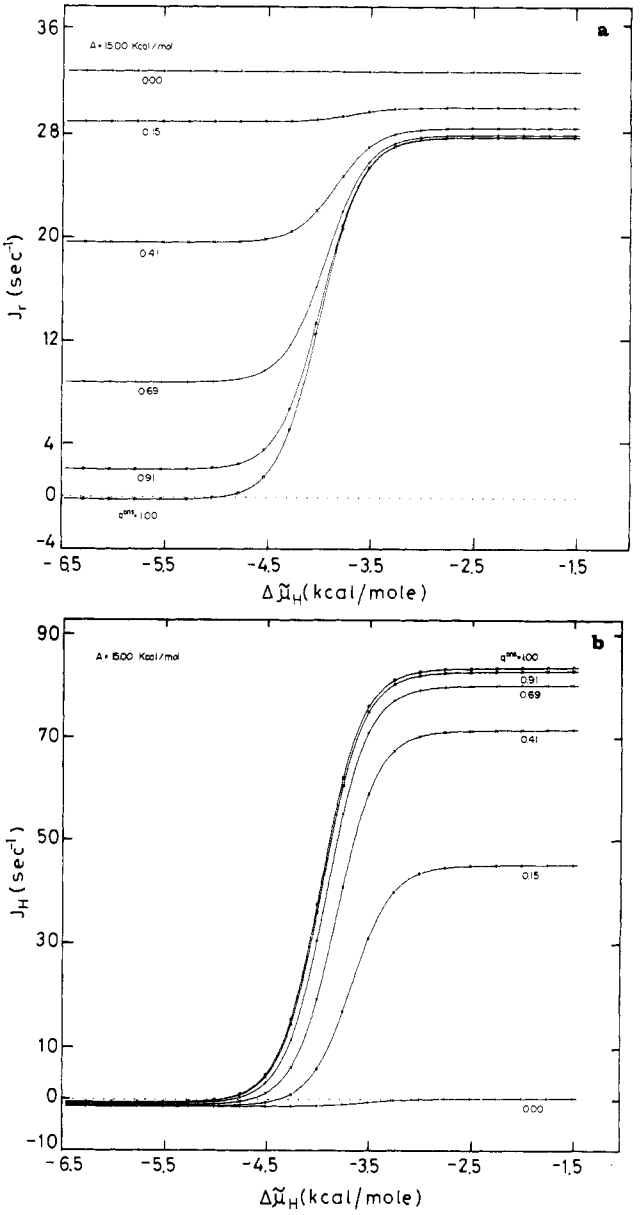

FIGURE 5: Flow–force relationships in the presence of intrinsic uncoupling for pump A at high fixed affinity. Families of curves correspond to increasing α_{52} and α_{25} (degree of coupling q^{ons} varies from 1 to 0). $\Delta\tilde{\mu}_H$ is varied by varying $\Delta\psi$. (a) J_r vs. $\Delta\tilde{\mu}_H$: reaction slip decreases as $|\Delta\tilde{\mu}_H|$ decreases. (b) J_H vs. $\Delta\tilde{\mu}_H$: proton slip is negligible; proton flux is reduced due to competition between cycles c and a.

dependence of J_H on $\Delta\tilde{\mu}_H$ above a threshold value. Figure 6a shows the decrease in the rate of ATP synthesis as a result of uncoupling. This decrease is not due to an increase in reaction slip, since at $q^{ons} \approx 0$ the reaction rate is virtually zero over the entire range of $\Delta\tilde{\mu}_H$. As before, it is due to the decreased probability of cycle a, which is now in competition with cycle b.

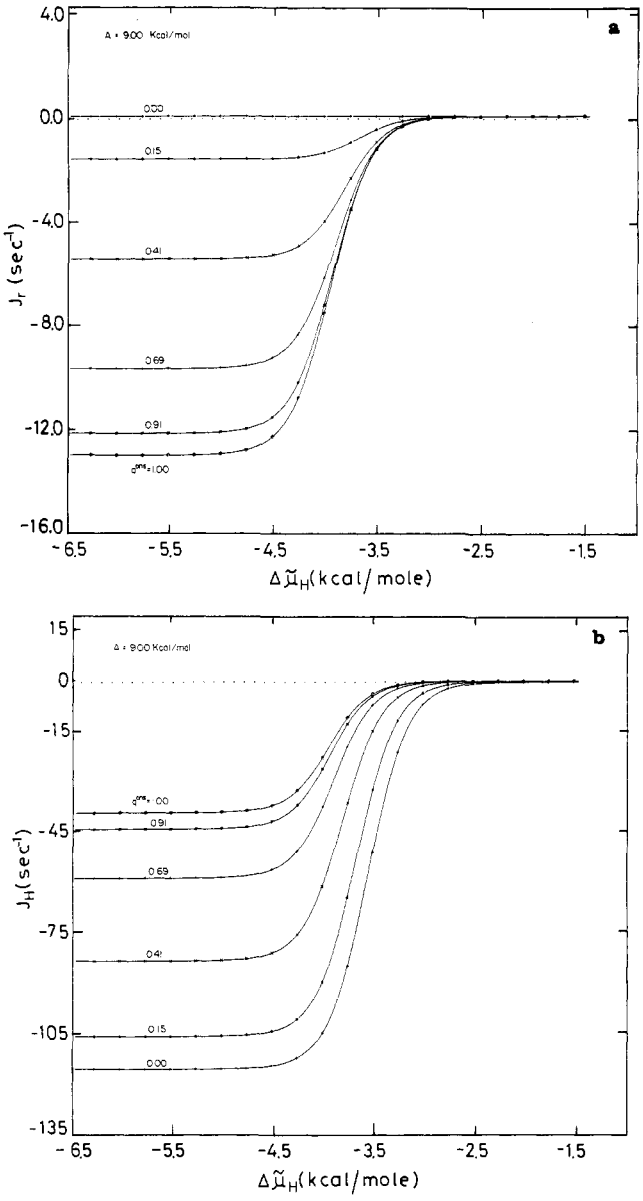

FIGURE 6: Flow–force relationships in the presence of intrinsic uncoupling for pump A at low fixed affinity. Families of curves correspond to increasing α_{52} and α_{25} (degree of coupling q^{ons} varies from 1 to 0). $\Delta\tilde{\mu}_H$ is varied by varying $\Delta\psi$. (a) J_r vs. $\Delta\tilde{\mu}_H$: reaction slip is negligible; ATP synthesis is decreased due to competition between cycles b and a. (b) J_H vs. $\Delta\tilde{\mu}_H$: proton slip is occurring, with steep dependence of J_H on $\Delta\tilde{\mu}_H$.

In conclusion, we may generalize by saying that increasing intrinsic uncoupling leads to an increased contribution to the input flow by the uncoupled cycle corresponding to the energy input, with a concomitant decrease in the contribution of the fully coupled cycle. The relative contributions of the cycles depend on the magnitude of the forces. In the case of pump A, operation at either high affinity or low affinity gives rise almost exclusively to reaction slip or proton slip, respectively, but at intermediate values of the affinity all possible cases of mixed slip can be found.

Analysis of the Linear Domain

(*a*) *Completely Coupled Pumps.* In this case, as we have seen, there is only one independent flow, since $J_H = nJ_r$. The driving force is $A + n\Delta\tilde{\mu}_H$. Near equilibrium, eq 4 and 5 become, respectively

$$J_r = (a^{eq}/RT)(A + n\Delta\tilde{\mu}_H) \quad (8)$$

$$J_H = (na^{eq}/RT)(A + n\Delta\tilde{\mu}_H) \quad (9)$$

where $a^{eq} = f_a(c_H^{in(eq)}, c_H^{ex(eq)}, c_S^{eq}, c_P^{eq}, \Delta\psi^{eq})$. Equations 8 and 9 exhibit characteristic Onsager symmetry, but it should be emphasized that they hold only when both $|A| \ll RT$ and $|n\Delta\tilde{\mu}_H| \ll RT$ or, more interestingly, when these forces have high values, yet their sum $|A + n\Delta\tilde{\mu}_H| \ll RT$. The latter condition defines an extremely restricted linear region in which A may be varied around its equilibrium value A^{eq} (i.e., the value at which the flows vanish) while maintaining $|\Delta\tilde{\mu}_H|$ ($=A^{eq}/n$) constant, or $\Delta\tilde{\mu}_H$ may be varied around its equilibrium value $\Delta\tilde{\mu}_H^{eq}$ while maintaining A ($=|n\Delta\tilde{\mu}_H^{eq}|$) constant. Indeed, the extent of the variations over which eq 8 and 9 hold will not exceed, say, ±0.01 kcal/mol. In comparison it can be seen that in the cases simulated in Figures 2a and 3a the approximately linear region of force control extends over roughly 0.6 (Figure 2a) or 0.5 kcal/mol (Figure 3a). The region of approximate linearity is more extended when the affinity is varied: it is about 1.5 kcal/mol in both Figure 2b and Figure 3b. The criterion for approximate linearity is that the values of the flows predicted from the tangent to the inflection point do not deviate by more than 10% from those given by the curve.

The regions of approximate linearity around an inflection point arbitrarily far from equilibrium can be described by empirical equations of the type (Rottenberg, 1973; van der Meer et al., 1980):

$$J_r = L_rA + L_{rH}\Delta\tilde{\mu}_H + K_r \quad (10)$$

$$J_H = L_{Hr}A + L_H\Delta\tilde{\mu}_H + K_H \quad (11)$$

Since coupling is complete, $L_{Hr} = nL_r$, $L_H = nL_{rH}$, and $K_H = nK_r$. These equations seem to imply that if either flow is found to be approximately linear in $\Delta\tilde{\mu}_H$ (over some measureable range) at any given value of A, then on fixing $\Delta\tilde{\mu}_H$ within that linear range, and varying A about its previously constant value, we should again find approximate linearity (over some measurable range). However, even if this can occur under certain conditions, it is not generally the case, as will be demonstrated below. Nonetheless, the restricted (Onsager) region described by eq 8 and 9 might possibly, in favorable circumstances, coincide with such an extended region of approximate linearity. The range of force control (for both forces) would then be centered on the equilibrium state. In such circumstances, eq 10 and 11 would reduce to eq 8 and 9, with $K_r = K_H = 0$, $L_r = a^{eq}/RT$, $L_{rH} = L_{Hr} = na^{eq}/RT$, and $L_H = n^2a^{eq}/RT$. On the other hand, as an example of the general case, consider curves b and h of Figure 2. The slopes of the tangents (dashed lines) to the equilibrium point, defined for both curves by A = 13.5 kcal/mol and $\Delta\tilde{\mu}_H$ = −4.5 kcal/mol, represent na^{eq} and a^{eq}, respectively. Clearly the slopes of the tangents (solid lines) to the inflection points, L_{rH} and L_r, respectively, are different. We can write

$$L_{rH} = L_H/n = \alpha na^{eq}/RT \quad (12)$$

$$L_r = L_{Hr}/n = \beta a^{eq}/RT \quad (13)$$

Equations 10 and 11 for the extended region then become

$$J_r = (a^{eq}/RT)(\beta A + \alpha n\Delta\tilde{\mu}_H) + K_r \quad (14)$$

$$J_H = (na^{eq}/RT)(\beta A + \alpha n\Delta\tilde{\mu}_H) + nK_r \quad (15)$$

where $\alpha = \alpha(A)$ and depends on the value of A held constant while $\Delta\tilde{\mu}_H$ is varied over an experimentally established linear range, while $\beta = \beta(\Delta\tilde{\mu}_H)$ and depends on the value of $\Delta\tilde{\mu}_H$ held constant while A is varied over an experimentally established linear range. Similarly, K_r depends on the particular values of A and $\Delta\tilde{\mu}_H$ around which a region of linearity is found.

These equations are similar to those suggested by van Dam et al. (1980):

$$J_r = L(A + \gamma n\Delta\tilde{\mu}_H) + K_r \quad (16)$$

$$J_H = nL(A + \gamma n\Delta\tilde{\mu}_H) + nK_r \quad (17)$$

where $L = \beta a^{eq}/RT$ and $\gamma = \alpha/\beta$.

Inspection of Figures 2 and 3 clarifies several aspects of the behavior of completely coupled pumps in terms of the parameters of eq 14 and 15. First, in general $\alpha \neq \beta$ (i.e., $L_{rH}/L_{Hr} = \alpha/\beta \neq 1$). This means that in general the two forces A and $\Delta\tilde{\mu}_H$ are kinetically inequivalent, so that equal changes in these forces have different impacts on the flow (van Dam et al., 1980; Westerhoff, 1983). Second, the condition $\alpha = \beta$ (or $\gamma = 1$), considered by van Dam et al. (1980) to be associated with equilibrium, occurs *only* at an MIP (which of course may be far from equilibrium). For example, compare curves b and f in Figure 3: here the forces characterizing the two curves ($A = 18.50$ kcal/mol, $\Delta\tilde{\mu}_H = -4.06$ kcal/mol) combine to give a state that is an inflection point of each curve. This is an MIP far from the equilibrium point of both curves. In this case, although as can be seen α and β are both very different from unity, $\alpha = \beta$ and the two forces are kinetically equivalent over the linear range. In Figure 2 we have an example of an MIP in which α and β are both close to, but not exactly, unity: curves c and f. Note that the closer the MIP is to equilibrium, the closer α and β are to unity and the smaller is the value of the additive constant K_r. On the other hand, if the equilibrium state is not an MIP, then even if it is within an extended range of linearity when $\Delta\tilde{\mu}_H$ is varied ($\alpha = 1$), in general $\beta \neq 1$ and hence $\gamma \neq 1$. A case in point is shown in Figure 3: curve d in Figure 3a should be compared with curve f in Figure 3b. The equilibrium point (defined by $A = 16.24$ kcal/mol and $\Delta\tilde{\mu}_H = -4.06$ kcal/mol) is in the linear region of curve d ($\alpha = 1$) and in the lower saturated region of curve f. An example of the reverse case also appears in Figure 3. Note that, for each α determined by the choice of A (when A is held constant), there is an infinite set of β's determined by the choice of $\Delta\tilde{\mu}_H$ (when $\Delta\tilde{\mu}_H$ is held constant), and vice versa. Symmetry is a sensitive function of the distance of A from its value at the MIP (if it exists) at a given $\Delta\tilde{\mu}_H$, and vice versa. From eq 12 and 13 one can formally write the parameters Z and q:

$$Z \equiv \sqrt{L_H/L_r} = n\sqrt{\alpha/\beta} \quad (18a)$$

$$q \equiv \sqrt{L_{Hr}L_{rH}/L_HL_r} = 1 \quad (18b)$$

Hence the phenomenological stoichiometry is a measure of the mechanistic stoichiometry only when $\alpha/\beta = 1$, i.e., at the MIP, even though the system is fully coupled. Away from the MIP, Z has no meaning. To determine n in completely coupled systems, the appropriate measure is, in general, not Z but L_H/L_{rH} (see eq 12). From the above observations it is clear that the phenomenological equations (10) and (11) are of limited use in analyzing experiments in which both A and $\Delta\tilde{\mu}_H$ are varied.

On the other hand, many studies have been carried out in different systems in which only one force is varied, while the other (usually A) is kept constant (or assumed to be constant). In this case the question of kinetic equivalence is irrelevant. Instead of eq 13 we can write

$$L_r = L_{Hr}/n = \alpha a^{eq}/RT \quad (A \text{ constant}) \quad (19)$$

and instead of eq 14 and 15 we have

$$J_r = (\alpha a^{eq}/RT)(A + n\Delta\tilde{\mu}_H) + K'_r \quad (A \text{ constant}) \quad (20)$$

$$J_H = (n\alpha a^{eq}/RT)(A + n\Delta\tilde{\mu}_H) + nK'_r \quad (A \text{ constant}) \quad (21)$$

Table II: Values of Effective Parameters Obtained by Variation in the Linear Range of One Force Only[a] for Several Illustrative Curves Taken from Figures 2 and 3[b]

figure	curve	$(L_{rH}/L_{Hr})^{eff}$	Z^{eff}	q_{Hr}^{eff}	q_{rH}^{eff}
2a (pump A)	a	1.14	3.20	0.94	1.07
	b	1.04	3.06	0.98	1.02
	c	1.00	3.00	1.00	1.00
	d	0.84	2.75	1.09	0.92
3a (pump B)	a	1.14	4.28	0.94	1.07
	b	1.07	4.13	0.97	1.03
	c	1.04	4.07	0.98	1.02
	d	1.00	4.00	1.00	1.00

[a] In this case, $\Delta\tilde{\mu}_H$. [b] Completely coupled pumps.

where K'_r is simply the intercept of the line J_r vs. $(A + n\Delta\tilde{\mu}_H)$. The symmetry that appears in eq 20 and 21 is entirely formal. However, if $\Delta\tilde{\mu}_H^{eq}$ is within the linear region (strictly speaking, at the inflection point) of J_r vs. $\Delta\tilde{\mu}_H$, $\alpha = 1$ and $K'_r = 0$. In general, it is useful (from the experimental point of view) to rewrite eq 20 and 21 in the form

$$J_r = \left(\frac{\alpha a^{eq}}{RT} + \frac{K'_r}{A}\right)A + n\left(\frac{\alpha a^{eq}}{RT}\right)\Delta\tilde{\mu}_H = L_r^{eff}A + L_{rH}^{eff}\Delta\tilde{\mu}_H \quad (22)$$

$$J_H = n\left(\frac{\alpha a^{eq}}{RT} + \frac{K'_r}{A}\right)A + n^2\left(\frac{\alpha a^{eq}}{RT}\right)\Delta\tilde{\mu}_H = L_{Hr}^{eff}A + L_H^{eff}\Delta\tilde{\mu}_H \quad (23)$$

remembering that A is constant. These four effective phenomenological coefficients are readily determined by measuring the slopes and intercepts of the linear ranges of the curves J_r and J_H vs. $\Delta\tilde{\mu}_H$ (Stucki, 1980b; Pietrobon et al., 1982; Caplan & Essig, 1983). From eq 22 and 23

$$\left(\frac{L_{rH}}{L_{Hr}}\right)^{eff} = \frac{1}{1+\delta} \qquad Z^{eff} = \frac{n}{\sqrt{1+\delta}}$$

$$q_{rH}^{eff} = \frac{1}{\sqrt{1+\delta}} \qquad q_{Hr}^{eff} = \sqrt{1+\delta} \quad (24)$$

where

$$\delta = \frac{RTK'_r}{\alpha a^{eq}A} \quad (25)$$

and $q_{rH}^{eff}q_{Hr}^{eff} = 1$. If $\Delta\tilde{\mu}_H^{eq}$ is within the range of extended linearity around the inflection point, as in the case of curve c of Figure 2a and curve d of Figure 3a, $(L_{rH}/L_{Hr})^{eff} = 1$ and $Z^{eff} = n$, i.e., $\delta = 0$ (see Table II). With increasing distance of $\Delta\tilde{\mu}_H^{eq}$ from the region of approximate linearity, i.e., as we move upward from curve c to curve a in Figure 2a or from curve d to curve a in Figure 3a, δ becomes increasingly negative due to the increasingly negative value of K'_r. Table II shows the consequences of this on the effective parameters when $\Delta\tilde{\mu}_H$ is the output force: as $\Delta\tilde{\mu}_H^{eq}$ becomes further removed from the linear region, $(L_{rH}/L_{Hr})^{eff}$, Z^{eff}, and q_{rH}^{eff} all increase while q_{Hr}^{eff} decreases. In these circumstances $(L_{rH}/L_{Hr})^{eff} > 1$ and $Z^{eff} > n$. However, it is seen in Table II that, even for curves a in Figures 2 and 3, $(L_{rH}/L_{Hr})^{eff}$ is not much greater than 1 and Z^{eff} is not much greater than n, i.e., $|\delta|$ is small. This may justify the use of proportional phenomenological equations as a good approximation for regions of extended linearity not containing the equilibrium point but sufficiently close to it.

(*b*) *Incompletely Coupled Pumps.* In this case there are two independent flows. The forces are A and $\Delta\tilde{\mu}_H$. Near

Table III: Values of Thermodynamic Parameters at the MIP for Two Pumps for Increasing Values of the Slip Transition Rate Constants[a]

pump	α_{52}	q^{ons}	q	Z^{ons}/n	Z/n	L_{rH}/L_{Hr}	K_r	K_H
A (Figure 2)	1×10^{-20}	1.00	1.00	1.00	1.00	1.00	−0.18	−0.54
	10	0.91	0.95	1.09	1.00	0.90	−11.10	−3.35
	50	0.69	0.80	1.38	1.00	0.64	−42.90	−12.6
	2×10^2	0.41	0.53	2.05	0.98	0.29	−94.30	−32.0
	10^3	0.15	0.22	3.26	0.91	0.06	−139.30	−57.0
B (Figure 3)	1×10^{-20}	1.00	1.00	1.00	1.00	1.00	−2.75	−11.0
	0.2	0.80	0.98	1.25	1.00	0.97	−4.53	−11.6
	1	0.51	0.91	1.93	0.98	0.87	−11.2	−13.9
	2	0.39	0.84	2.53	0.95	0.77	−18.6	−16.4
	10	0.18	0.56	5.09	0.86	0.43	−55.8	−27.6

[a] The ratio α_{52}/α_{25} remains constant. The ranges of the forces are as follows: A(MIP) = 12.39 kcal/mol, $\Delta\tilde{\mu}_H$(MIP) = −3.98 kcal/mol (pump A, q^{ons} = 1.00); A(MIP) = 12.38 kcal/mol, $\Delta\tilde{\mu}_H$(MIP) = −3.69 kcal/mol (pump A, q^{ons} = 0.15); A(MIP) = 18.50 kcal/mol, $\Delta\tilde{\mu}_H$(MIP) = −4.06 kcal/mol (pump B, q^{ons} = 1.00); A(MIP) = 18.76 kcal/mol, $\Delta\tilde{\mu}_H$(MIP) = −3.92 kcal/mol (pump B, q^{ons} = 0.18).

equilibrium, when both forces are very small, eq 6 and 7 become

$$J_r = [(a^{eq} + c^{eq})/RT]A + [na^{eq}/RT]\Delta\tilde{\mu}_H \quad (26)$$

$$J_H = [na^{eq}/RT]A + [n^2(a^{eq} + b^{eq})/RT]\Delta\tilde{\mu}_H \quad (27)$$

where all three kinetic coefficients a^{eq}, b^{eq}, and c^{eq} are functions of the equilibrium values of all the concentrations and $\Delta\psi$ (see Appendix 2). Equations 26 and 27, like eq 8 and 9, exhibit Onsager symmetry, but in this case the exclusive condition that they hold is that both $|A| \ll RT$ and $|n\Delta\tilde{\mu}_H| \ll RT$. We designate this region the "Onsager domain": its extent, for both A and $n\Delta\tilde{\mu}_H$, is in general roughly 0 ± 0.01 kcal/mol. The thermodynamic parameters for the Onsager domain are (Caplan, 1981)

$$q^{ons} = [(1 + b^{eq}/a^{eq})(1 + c^{eq}/a^{eq})]^{-1/2} \quad (28)$$

$$Z^{ons} = n[(1 + b^{eq}/a^{eq})/(1 + c^{eq}/a^{eq})]^{1/2} \quad (29)$$

Thus q^{ons} and Z^{ons} are fundamental characteristics of the pump.

It is of interest to examine the effect of increasing intrinsic uncoupling on the parameters q and Z measured in the extended range of linearity around an MIP and also on the parameters q^{eff} and Z^{eff} obtained by variation of one force only (in a linear range), the other being held constant. An empirical representation of the range of linearity in the neighborhood of an MIP is given by eq 10 and 11, where $L_{Hr} = L_{rH}$. The quantities q and Z may again be defined for this region as

$$q \equiv L_{Hr}/(L_r L_H)^{1/2} \quad (30)$$

$$Z \equiv (L_H/L_r)^{1/2} \quad (31)$$

[explicit expressions for the L's in the case of a five-state model have been derived previously (Caplan, 1981)]. Table III shows how these and other thermodynamic parameters vary at the MIP for pumps A and B when the rate constants of the slip transition are increased while maintaining their ratio constant. It is seen that in general q deviates very markedly from q^{ons} toward higher values and may be quite close to unity even at low q^{ons}. This effect becomes larger as the MIP moves further away from the equilibrium point of the fully coupled cycle ($A + n\Delta\tilde{\mu}_H = 0$). For example, compare pump A, where the MIP is close to the equilibrium point of the fully coupled cycle, with pump B, where the MIP is further from the equilibrium point. Table III also shows that while Z^{ons}/n increases rather rapidly with decreasing q^{ons}, Z/n measured at the MIP *decreases* from the value of unity at q^{ons} = 1, but rather slowly. The opposite directions of change in Z^{ons}/n and Z/n suggest that at very low values of the forces cycle b predominates in bringing about slip, while at higher values of the forces cycle c starts to predominate (see below). It can be seen from Table III that uncoupling introduces asymmetry: with decreasing q^{ons} the ratio L_{rH}/L_{Hr} falls from the value of unity at q^{ons} = 1. Note that both K_H and K_r become increasingly more negative as q^{ons} decreases (their values at q^{ons} = 1 depend, of course, on the distance of the MIP from the point of equilibrium). K_r increases in absolute value much more rapidly than K_H.

Table IV: Values of Effective Parameters Obtained from Slopes and Intercepts by Variation of One Force Only in the Linear Range, for Pump B with Increasing Intrinsic Uncoupling[a]

q^{ons}	$(L_{rH}/L_{Hr})^{eff}$	q_{Hr}^{eff}	q_{rH}^{eff}	Z^{eff}	$(L_H/L_{rH})^{eff}$
1.00	1.14	0.94	1.07	4.28	4.00
0.80	1.13	0.94	1.06	4.31	4.05
0.51	1.07	0.96	1.03	4.41	4.28
0.45	1.05	0.97	1.02	4.46	4.39
0.39	1.01	0.98	0.99	4.53	4.55
0.18	0.68	1.14	0.78	5.33	6.83
0.12	0.48	1.28	0.62	6.06	9.79

[a] $\Delta\tilde{\mu}_H$ is varied while A is constant at 10.66 kcal/mol.

The influence of increasing intrinsic uncoupling on the phenomenological parameters obtained from the slopes and intercepts when one force is varied in a linear range while the other is kept constant is shown in Table IV for pump B. In this case, as in the completely coupled case, it is convenient to introduce effective coefficients. Assuming A is held constant

$$L_r^{eff} = L_r + K_r/A \qquad L_{Hr}^{eff} = L_{Hr} + K_H/A$$

$$L_{rH}^{eff} = L_{rH} \qquad L_H^{eff} = L_H \quad (32)$$

The ratio $(L_{rH}/L_{Hr})^{eff}$ for q^{ons} = 1 is higher than 1 because the equilibrium value of $\Delta\tilde{\mu}_H$, $\Delta\tilde{\mu}_H^{eq}$, is not in the extended region of linearity (the further the linear region from this value, the higher the ratio). Table IV indicates that the ratio decreases with increasing uncoupling. Hence we find that increasing uncoupling can lead to apparent symmetry, by mutual compensation of the two effects, at $q^{ons} < 1$. This compensation is also seen in the behavior of q_{rH}^{eff} and q_{Hr}^{eff}, where an apparent complete coupling is found at a value of $q^{ons} < 1$. The parameter Z^{eff} always increases with increasing uncoupling. Note that the ratio $(L_H/L_{rH})^{eff}$ ($=L_H/L_{rH}$), which always has the value n at q^{ons} = 1, increases with uncoupling even more rapidly than Z^{eff}.

Discussion and Conclusions

Sigmoidal flow–force relationships are a general characteristic of models of ion pumps or cotransport systems involving cyclic reaction schemes with one voltage-dependent step (Hansen et al., 1981; Chapman et al., 1983; Kishimoto et al., 1984). This characteristic is not conditional on the reaction sequence or on the position in this sequence of the step chosen to be voltage dependent (Chapman et al., 1983). Sigmoidal relationships have also been observed experimentally (Nicholls & Bernson, 1977; Gräber, 1982; van den Berg et al., 1982; Wanders et al., 1982). Indeed the typical relationship between

Table V: Values of Effective Parameters for Pumps with Regions of Approximate Linearity Increasingly Far from Equilibrium: Comparison with Experimental Effective Parameters of Mitochondrial Redox Proton Pumps[a]

	$(L_{rH}/L_{Hr})^{eff}$	q_{Hr}^{eff}	q_{rH}^{eff}	Z^{eff}	$(L_H/L_{rH})^{eff}$	$(A/n\|\Delta\tilde{\mu}_H\|)^{sh}$	η_{max}
			Simulations				
1 (Figure 4)	1.14	0.94	1.07	4.28	4.00	1.00	1.00
leak	1.14	0.93	1.06	4.32	4.08	1.15	0.65
leak + slip	1.05	0.97	1.01	4.47	4.41	1.11	0.70
2a (Figure 4)	1.32	0.87	1.15	4.60	4.00	1.00	1.00
leak	1.32	0.85	1.13	4.69	4.15	1.32	0.51
leak + slip	1.21	0.89	1.08	4.78	4.44	1.22	0.53
3a (Figure 4)	1.62	0.79	1.27	5.09	4.00	1.00	1.00
leak	1.62	0.77	1.25	5.19	4.15	1.59	0.42
leak + slip	1.49	0.80	1.19	5.27	4.44	1.45	0.42
			Experiments				
succinate	1.11	0.94	1.03	4.34	4.21		
	1.04	0.92	0.96	4.22	4.38		
β-hydroxybutyrate	1.16	0.90	1.05	6.18	5.90		
	1.10	0.93	1.03	6.20	6.04		
	1.25	0.83	1.05	6.14	5.86		

[a] The values in the first row of each block under Simulations are calculated from curves 1, 2a, and 3a of Figure 4 with $n = 4$. The values in the subsequent rows are calculated with the same set of rate constants after introducing an appropriate proton leak in parallel, without or with intrinsic uncoupling (see Discussion and Conclusions). The experimental values are recalculated from Pietrobon et al. (1982). Recently, our determinations of $\Delta\tilde{\mu}_H$ have been improved with respect to both the measurement of the mitochondrial inner volume and the correction for binding of the probe used to measure $\Delta\psi$. Accordingly, all values of $\Delta\tilde{\mu}_H$ have been decreased by 0.8 kcal/mol. Two experiments are presented for electron transfer from succinate to oxygen and three for electron transfer from β-hydroxybutyrate to oxygen.

rate of ATP synthesis and $\Delta\tilde{\mu}_H$, characterized by a threshold value of $|\Delta\tilde{\mu}_H|$ below which no ATP synthesis occurs (Baccarini Melandri et al., 1977; Junge, 1970; Hangarter & Good, 1982; Maloney, 1982; Zoratti et al., 1982; Clark et al., 1983; McCarthy & Ferguson, 1983), resembles curve d in Figure 2a. It may therefore be, in principle, a simple consequence of the kinetic properties of the enzyme. Depending on the value of the affinity ("ΔG_p"), the generally kinetically reversible pump can behave as if it were kinetically irreversible. Hence it is quite likely that at least some cases of kinetic irreversibility are attributable to sigmoidicity in an appropriate range of the flows and forces, as has been suggested by Hansen et al. (1981). Gating effects, observed, for example, in the conductance of F_0, may be predicted from the regions of saturation. This is readily seen on examination of the curve for $q^{ons} = 0$ in Figure 6b. However, in chloroplasts, in contrast to curve a in Figure 2a, ATP hydrolysis is not observed even at high ΔG_p and low $|\Delta\tilde{\mu}_H|$ unless the enzyme is first activated by light or by an appropriate reducing agent. It has been suggested that activation may be induced directly by $\Delta\tilde{\mu}_H$ via a number of plausible mechanisms (Gräber, 1982; Mills & Mitchell, 1984). Analogous phenomena may well be present in mitochondria, where $\Delta\tilde{\mu}_H$ quite probably regulates the binding of the ATPase inhibitory protein (Power et al., 1983; Tuena de Gomez Puyou et al., 1983).

Linear relationships between flows and forces have equally often been found experimentally (see the introduction). In the case of the mitochondrial proton pumps these relationships very probably correspond to the regions of approximate linearity around inflection points analyzed in this study. Our results indicate that the application of the linear phenomenological equations of near-equilibrium NET to such regions is at best a simplification to be treated with great caution. The values of q and Z that have been reported for mitochondrial proton pumps are for the most part effective values (Rottenberg, 1979; Stucki, 1980b; Pietrobon et al., 1982; Lemasters et al., 1984). As can be seen in Table IV, they are not simply related to q^{ons} and Z^{ons}, and in the absence of independent information regarding the distance from equilibrium of the flow-controlling ranges of the forces (i.e., how far from equilibrium the pumps normally operate) they give very little information about the degree of coupling and the mechanistic stoichiometry. In fact, their values [as well as the value $\gamma_0 n_H^0$ in van Dam et al. (1980), which corresponds to our $n/(1 + \delta)$] are essentially governed by the position of the extended region of approximate linearity relative to the equilibrium point. This is seen more clearly in Table V. The effective values in the first rows of each block are calculated from the slopes and intercepts of the linear regions of the three curves 1, 2a, and 3a of Figure 4. These represent a completely coupled case (no slip or leak). On going from curve 1 to curve 3a, Z^{eff} increasingly overestimates n, and q_{rH}^{eff} and q_{Hr}^{eff} increasingly deviate from 1 ($q_{rH}^{eff} > 1$, $q_{Hr}^{eff} < 1$). An experimental determination of the symmetry parameter $(L_{rH}/L_{Hr})^{eff}$ does, however, give an idea of how far from equilibrium the pumps are actually operating, since it becomes progressively larger than 1 as this distance increases. It should be noted that a finding that $(L_{rH}/L_{Hr})^{eff} \approx 1$ (Stucki, 1980b; Pietrobon et al., 1982) does not necessarily mean that the region of linearity considered is centered on equilibrium and that it coincides with the Onsager domain. Nevertheless, for completely coupled pumps one can safely assume in this case that the region of linearity is not far from equilibrium, and hence Z^{eff} and q_{rH}^{eff} are not much greater than n and 1, respectively.

The real system, however, cannot manifest complete coupling between electron flow and proton flow because the membrane has a finite permeability to protons and there are slips in the pumps (Pietrobon et al., 1981, 1983; Zoratti et al., 1984). In this regard, recent measurements of passive proton influx in mitochondria at a value of $\Delta\tilde{\mu}_H$ corresponding to static head, compared with values for the electron flow from succinate to oxygen at static head, lead to the following conclusion: assuming $n = 4$ H^+/e in this case, only about 30% of the electron flow at static head is accounted for by parallel leaks (Zoratti et al., unpublished experiments). Quantitative analysis of the data of Krishnamoorthy & Hinkle (1984) leads to a similar conclusion. We have simulated the addition of a proton leak (comparable to the one observed) in parallel with the pump characterized by curve 1, Figure 4, which has flow-controlling ranges of $\Delta\tilde{\mu}_H$ and values of the flows and of $(L_{rH}/L_{Hr})^{eff}$ close to those determined experimentally (Pietrobon et al., 1982). The proton leak was combined with an

intrinsic uncoupling such that together the leak and slip account for the electron transport at static head in the above-mentioned proportions. This has enabled us to reproduce all the results of titrations with inhibitors of electron flow at static head (Pietrobon et al., 1981, 1983) and analogous results obtained by varying the succinate concentration (Pietrobon et al., unpublished experiments). Table V shows the effect of introducing the leak and slip, as described, on the effective parameters. It is worthwhile noting that the direction in which these parameters vary when intrinsic uncoupling is introduced is independent of the relative contributions of the two uncoupled cycles b and c (although the magnitude of the variation depends on these contributions).

The most informative parameter with respect to the mechanistic stoichiometry n is $(L_H/L_{rH})^{eff}$. It is always equal to n in the completely coupled case no matter how far from equilibrium the pump may operate, and it is not grossly higher than n in the case of a reasonable degree of uncoupling (indeed, if the uncoupling is solely due to a modest parallel leak, it may be very slightly higher than n). Inspection of Table V indicates that the parameters determined for the mitochondrial redox pumps (Pietrobon et al., 1982) yield the following consistent picture: $n = 4$ and $q < 1$ for electron transfer from succinate to oxygen, and $n = 6$ and $q \approx 1$ for electron transfer from β-hydroxybutyrate to oxygen. The flow-controlling ranges of $\Delta\tilde{\mu}_H$ are not far from equilibrium in either case, since the symmetry parameter is close to unity. A word of caution is, however, necessary. These conclusions are highly dependent on the correctness of the determination of $\Delta\tilde{\mu}_H$ and, especially, of the electron flow. If for some reason the latter is underestimated by, say, 15%, the same data on comparison with the simulated behavior would lead to a different picture: for electron transfer to oxygen from succinate $n = 3$, and for transfer from β-hydroxybutyrate $n = 5$. Furthermore, the flow-controlling ranges of $\Delta\tilde{\mu}_H$ are now far from equilibrium, since $(L_{rH}/L_{Hr})^{eff} = 1.3$–$1.4$.

A knowledge of the distance from equilibrium of the flow-controlling ranges of the forces is also crucial for the interpretation of measurements of force ratios at static head. Table V shows that, for a given degree of uncoupling, the extent to which the ratio of input to output force at static head overestimates the mechanistic stoichiometry increases as the flow-controlling ranges of $\Delta\tilde{\mu}_H$ move further from equilibrium. If, however, uncoupling were entirely intrinsic (no parallel leaks) this ratio would always remain close to n (Caplan, 1981).

Useful relationships have been derived (Kedem & Caplan, 1965) describing the static head force ratio and the maximum efficiency of energy conversion in the Onsager domain: $|X_1/X_2|^{sh} = q^{ons}/Z^{ons}$ (where X_1 and X_2 are the output and input forces, respectively), and $\eta_{max} = (q^{ons})^2/[1 + [1 - (q^{ons})^2]^{1/2}]^2$. Unfortunately, these relations do not hold for the extended regions of linearity at physiological (i.e., high) values of the forces—even on replacing the Onsager parameters by q^{eff} and Z^{eff}, or by q(MIP) and Z(MIP). Indeed, a low static head force ratio does not necessarily indicate a low degree of coupling of the pump and/or low maximal efficiency; rather, it suggests the presence of a leak in parallel with a pump operating far from equilibrium. However, as is seen in Table V, the more the flow-controlling ranges of the output force are removed from equilibrium, the lower the maximal efficiency. It is worth noting that in all cases $\eta_{max} > \eta_{max}^{ons}$. [This conclusion is opposite to that reached by Stucki et al. (1983). See Appendix 2 for discussion.] For active proton pumping (high values of A) there is a buffering of η_{max}: over a wide range changes in q^{ons} produce relatively small changes in η_{max}. An interesting observation is that the relationship describing the level flow ratio of flows in the Onsager domain continues to hold *exactly*, irrespective of the direction of pumping, even far from equilibrium (Caplan, 1981). If the forces could separately be clamped by some means at the value zero, q^{ons} and Z^{ons} could in principle be measured directly, since $[(J_H/J_r)_{\Delta\tilde{\mu}_H=0}(J_r/J_H)_{A=0}]^{1/2} = q^{ons}$ and $[(J_H/J_r)_{\Delta\tilde{\mu}_H=0}/(J_r/J_H)_{A=0}]^{1/2} = Z^{ons}$. However, these values cannot be used in any simple way to predict maximal efficiency far from equilibium, since the latter depends on the magnitude of the forces. Furthermore, the effective degree of coupling measured far from equilibrium itself depends on the magnitude of the forces.

When regions of linearity with respect to both input and output forces are studied, meaningful parameters q and Z can be obtained from the slopes of the flow–force curves only if the pump is operating in the vicinity of an MIP. However, these parameters are again not simply related to q^{ons} and Z^{ons}, and the typical relationships of the Onsager domain do not hold. In the completely coupled case symmetrical equations can be used, symmetry being a manifestation of kinetic equivalence between input and output forces that occurs only in the Onsager domain and at all MIP's. Far from the MIP the more general equations (10) and (11) must be used. Rottenberg (1973) demonstrated a range of linearity in both forces, as well as symmetry, in a study of oxidative phosphorylation in intact mitochondria. His results suggest that the mitochondria were functioning close to an MIP, but it should be remembered this is a system of greater complexity than those we have been considering, since two pumps are involved linked in series.

Complex systems may well give rise to new phenomena. It may be noted that extensive studies of active ion transport in epithelial membranes have been reported, based on the use of linear NET (Caplan & Essig, 1983). These studies all depend on the determination of effective parameters, since the only force that can be varied systematically is the electrochemical potential difference of the transported ion across the membrane. Independent evidence exists for the constancy of the other force under these conditions (Civan et al., 1983). The flows measured are the ion flux and the respiration rate (as reflected in O_2 consumption or CO_2 production). Epithelial systems show remarkably broad ranges of linearity, sometimes extending over 4–5 kcal/mol, which generally include static head. Since they are extremely complex as compared with the model we have been studying, it is not clear to what extent the model results apply, if at all. At any rate the generally made assumption of symmetry, which is required in order to calculate the affinity of the driving reaction from the effective parameters, is a good approximation if the system operates close to equilibrium.

Some degree of slip, however slight, may be inevitable in any pump mechanism. However, intrinsic uncoupling may actually play an important regulatory role in the operation of the pump, for example, in fine tuning the pumping rate or in matching the pump to the load for optimalization purposes as suggested by Stucki (1980b). Thus there may be physiological effectors that bind to the pump and act to regulate the slip. Regulation of the slip by the forces is, as we have shown, a characteristic of models of this type that may well have physiological significance. In general, the forces determine both the relative contributions and the magnitudes of the uncoupled cycles. To the extent that the contribution of one or the other uncoupled cycle is increased, the contribution of

the fully coupled cycle is decreased due to the competition between them. Physiologically significant aspects of this regulation are (1) the steep dependence of the proton slip on $\Delta\tilde{\mu}_H$ and its sharp cutoff below a threshold value (see Figure 6b) and (2) the regulation by $\Delta\tilde{\mu}_H$ of the reaction slip as well, which decreases as $|\Delta\tilde{\mu}_H|$ decreases. When an increased rate of phosphorylation is needed, and consequently $\Delta\tilde{\mu}_H$ is decreased, the contributions of both the reaction slip cycle of the redox pumps and the proton slip cycle of the ATP synthase pumps decrease while the contributions of the coupled cycles of both pumps increase, thus increasing the overall degree of coupling and the efficiency of energy transduction. Regulation of intrinsic uncoupling by the forces in the photocycle of bacteriorhodopsin has been suggested by Caplan (1982), who pointed out that slip might provide a "safety valve" since the photoreaction proceeds at an essentially fixed rate, and by Westerhoff & Dancsházy (1984) for similar reasons. Recent studies by Dancsházy et al. (1984) apparently confirm the occurrence of a $\Delta\tilde{\mu}_H$-controlled slip regulation.

Appendix

(1) Reduction of a Diagram. The following is a brief outline of the reduction procedure used to eliminate explicit consideration of transient intermediates. The general approach has been described by Hill (1977). Consider the binding of four protons in transitions 1–2 or 6–5:

$$\overset{1}{\cdot}\ \underset{\alpha'_{21}}{\overset{\alpha'_{12}}{}}\ \underset{E}{\cdot}\ \underset{k_{21}}{\overset{4k_{12}c_H}{}}\ \underset{E'}{\cdot}\ \underset{2k_{21}}{\overset{3k_{12}c_H}{}}\ \underset{E'H}{\cdot}\ \underset{3k_{21}}{\overset{2k_{12}c_H}{}}\ \underset{E'H_2}{\cdot}\ \underset{4k_{21}}{\overset{k_{12}c_H}{}}\ \underset{E'H_3}{\cdot}\ \underset{\alpha''_{21}}{\overset{\alpha''_{12}}{}}\ \underset{E'H_4}{\cdot}\ \overset{2}{\underset{EH_4}{\cdot}}$$

In this scheme, four equivalent and independent binding sites for protons are postulated with binding constants given by the expression

$$\frac{\nu}{P-\nu+1}\frac{k_{12}}{k_{21}}$$

where ν is the number of free binding sites and P the total number of binding sites. In order to be able to treat the states E′, E′H, E′H_2, E′H_3, and E′H_4 as transient intermediates, a number of possible constraints may be imposed on the rate constants. Among these we choose the condition

$$\alpha'_{12},\ \alpha''_{21} \ll k_{21},\ \alpha'_{21} \qquad \text{(A1-1)}$$

The rate constants for the reduced transition are

$$\alpha_{12} = \frac{24\alpha'_{12}\alpha''_{12}(k_{12}c_H)^4}{\Phi}, \quad \alpha_{21} = \frac{24(k_{21})^4\alpha'_{21}\alpha''_{21}}{\Phi} \qquad \text{(A1-2)}$$

where

$$\Phi = 24\alpha''_{12}(k_{12}c_H)^4 + 6\alpha''_{12}\alpha'_{21}(k_{12}c_H)^3 + 2\alpha''_{12}\alpha'_{21}(k_{12}c_H)^2k_{21} + 2\alpha''_{12}\alpha'_{21}(k_{12}c_H)k_{21}^2 + 6\alpha''_{12}\alpha'_{21}k_{21}^3 + 24\alpha'_{21}k_{21}^4$$

The expressions in eq A1-2 may be conveniently rewritten in the form

$$\alpha_{12} = \frac{\alpha'_{12}\alpha''_{12}(k_{12}c_H)^4}{k_{21}^4\alpha'_{21}\Phi'}, \quad \alpha_{21} = \frac{\alpha''_{21}}{\Phi'} \qquad \text{(A1-3)}$$

where

$$\Phi' = 1 + \frac{\alpha''_{12}}{4k_{21}} + \frac{\alpha''_{12}k_{12}c_H}{12k_{21}^2} + \frac{\alpha''_{12}(k_{12}c_H)^2}{12k_{21}^3} + \frac{\alpha''_{12}(k_{12}c_H)^3}{4k_{21}^4} + \frac{\alpha''_{12}(k_{12}c_H)^4}{\alpha'_{21}k_{21}^4} \qquad \text{(A1-4)}$$

The condition for the reduction (A1-1) determines upper limits for the values of the reduced rate constants α_{12} and α_{21}, which depend on the values of the elementary rate constants and on the concentration of protons. Consider as an example the following case. If

$$\frac{\alpha''_{12}}{4k_{21}} \le 10^{-1}, \quad \frac{k_{12}c_H}{k_{21}} \approx 1, \quad \frac{\alpha''_{12}}{\alpha'_{21}} \le 1 \qquad \text{(A1-5)}$$

it follows that $\Phi' \approx 1$, and we have from eq A1-1, -3, and -5

$$\alpha_{12} \ll 10^{-1}(4k_{21}), \quad \alpha_{21} \ll k_{21} \qquad \text{(A1-6)}$$

The conditions (A1-6) are sufficiently well satisfied by

$$\alpha_{12} \le 10^{-2}(4k_{21}), \quad \alpha_{21} \le 10^{-1}(k_{21}) \qquad \text{(A1-7)}$$

If the upper limit of c_H is taken as $10^{-6.4}$ and $k_{12} = 10^{11}$, then from eq A1-5 $k_{21} = 4 \times 10^4$. Hence we may take

$$\alpha_{12} \le 1.6 \times 10^3, \quad \alpha_{21} \le 4 \times 10^3 \qquad \text{(A1-8)}$$

The transition 3–4 is treated similarly. In this case there is only one transient state between two serial transitions involving the successive release of products P_1 and P_2 ($P_1 = P_i$ or H^+, P_2 = ADP or fumarate). The condition for reduction poses constraints on the values that both reduced rate constants α_{34} and α_{43} can assume, depending on the values of the elementary rate constants and the concentrations of the products c_{P_1} and c_{P_2}.

(2) Cycle Fluxes. Intuitively, the cycle fluxes associated with a Hill diagram represent the net number of cycles of a given kind (a, b, or c) completed in unit time by an ensemble of N enzyme molecules (the net number of cycles being given by the difference between the numbers of cycles completed in the forward and backward directions). Explicitly, for any cycle κ of a given reaction scheme catalyzed by the ensemble, the cycle flux has the form

$$J_\kappa = N(\Pi_{\kappa^+} - \Pi_{\kappa^-})\Sigma_\kappa/\Sigma \qquad \text{(A2-1)}$$

where Π_{κ^+} and Π_{κ^-} are the products of the first-order or pseudo-first-order rate constants around the cycle in the anticlockwise (forward) or clockwise (backward) directions, respectively. Σ and Σ_κ are functions of the rate constants (Σ is a function of all the rate constants of the diagram, first order or pseudo first order, and hence of all the concentrations and $\Delta\psi$). Both Σ and Σ_κ may be written down by inspection of the diagram—the former in our case is a sum of 90 terms representing the so-called "directional diagrams" (Hill, 1977). Certain relationships between these terms determine the presence of an MIP (Rothschild et al., 1980; Caplan, 1981). Each transition flux J_{ij}, i.e., the net flow in the stationary state between states i and j, can be expressed as an algebraic sum of the cycle fluxes of all cycles that include the transition i–j. Hence

$$J_{23} = J_{34} = J_{45} = J_r = J_a + J_c \qquad \text{(A2-2)}$$

$$J_{12} = J_{61} = J_{56} = J_H/n = J_a + J_b \qquad \text{(A2-3)}$$

The cycle fluxes are readily expressed as functions of the respective thermodynamic forces driving the cycles, since as a consequence of the principle of microscopic reversibility, we have for any stationary state

$$(\Pi_{\kappa^+}/\Pi_{\kappa^-}) = e^{X_\kappa/RT} \qquad \text{(A2-4)}$$

Equations A2-1–A2-4 lead directly to eq 6 and 7, where the coefficients have the structure [cf. Caplan (1981)]:

$$a = (A/\Sigma')c_P(c_H^{ex})^n \qquad \text{(A2-5)}$$

$$b = (B/\Sigma')(c_H^{ex})^n \qquad \text{(A2-6)}$$

$$c = (C/\Sigma')(G + e^{n\Delta\tilde{\mu}_H/RT})c_P(c_H^{ex})^n \qquad \text{(A2-7)}$$

Here A, B, and C are constants (i.e., they are functions only of the true rate constants, the phase-boundary potentials, and

the invariant concentrations c_H^{in} and c_P), $\Sigma' = \Sigma(c_H^{in})^n e^{nF\Delta\psi/2RT}$, and G is given by

$$G = \frac{\alpha_{16}(0)\alpha_{65}}{\alpha_{61}(0)\alpha_{12}} \frac{(c_H^{in})^n}{(c_H^{ex})^n} \frac{e^{nF\Delta\psi_b^{ex}/RT}}{e^{nF\Delta\psi_b^{in}/RT}} \left(\frac{\alpha_{12}}{\alpha_{16}(0)} e^{nF\Delta\psi/2RT} + 1 \right) \quad \text{(A2-8)}$$

This quantity, which in our simulations must have a value in the range of 10^{-6}–10^{-9} to reproduce the experimentally observed flow–force curves, is related to (and plays the same role as) the factor γ introduced by Essig & Caplan (1981), Caplan (1981), and Stucki et al. (1983) for the case of a five-state model. Stucki and co-workers assumed that their factor γ would not fall below about 10^{-3} under physiological conditions and would generally have a considerably higher value. This led them to the conclusion that η_{max}^{ons} would normally greatly exceed η_{max}. However, in our simulations the opposite is the case.

Registry No. H^+, 12408-02-5.

REFERENCES

Azzone, G. F., Pozzan, T., Massari, S., Bragadin, M., & Pregnolato, L. (1978a) *Biochim. Biophys. Acta 501*, 296–306.

Azzone, G. F., Pozzan, T., & Massari, S. (1978b) *Biochim. Biophys. Acta 501*, 307–316.

Baccarini Melandri, A., Casadio, R., & Melandri, B. A. (1977) *Eur. J. Biochem. 78*, 389–402.

Caplan, S. R. (1971) *Curr. Top. Bioenerg. 4*, 1–65.

Caplan, S. R. (1981) *Proc. Natl. Acad. Sci. U.S.A. 78*, 4314–4318.

Caplan, S. R. (1982) in *Dynamic Aspects of Biopolyelectrolytes and Biomembranes* (Oosawa, F., Ed.) pp 431–441, Kodansha, Tokyo.

Caplan, S. R., & Essig, A. (1983) *Bioenergetics and Linear Nonequilibrium Thermodynamics: The Steady State*, Harvard University Press, Cambridge, MA.

Chapman, J. B., Johnson, E. A., & Kootsey, J. M. (1983) *J. Membr. Biol. 74*, 139–153.

Civan, M. M., Peterson-Yantorno, K., DiBona, D. R., Wilson, D. F., & Erecińska, M. (1983) *Am. J. Physiol. 245*, F691–F700.

Clark, A. J., Cotton, N. P. J., & Jackson, J. B. (1983) *Biochim. Biophys. Acta 723*, 440–453.

Dancshâzy, Zs., Groma, G. I., & Oesterhelt, D. (1984) *EBEC Reports 3A*, 229–230.

Dixon, T. E., & Al-Awqati, Q. (1979) *Proc. Natl. Acad. Sci. U.S.A. 76*, 3135–3138.

Eddy, A. A. (1980) *Biochem. Soc. Trans. 8*, 271–272.

Essig, A., & Caplan, S. R. (1981) *Proc. Natl. Acad. Sci. U.S.A. 78*, 1647–1651.

Fröhlich, O., Leibson, C., & Gunn, R. B. (1983) *J. Gen. Physiol. 81*, 127–152.

Geck, P., & Heinz, E. (1976) *Biochim. Biophys. Acta 443*, 49–53.

Gräber, P. (1982) *Curr. Top. Membr. Transp. 16*, 215–245.

Gräber, P., & Witt, H. T. (1976) *Biochim. Biophys. Acta 423*, 141–163.

Gräber, P., & Schlodder, E. (1981) in *Photosynthesis II. Electron Transport and Photophosphorylation* (Akoyunoglou, G., Ed.) pp 867–879, Balaban International Science Services, Philadelphia.

Grubmeyer, C., Cross, R. L., & Penefsky, H. S. (1982) *J. Biol. Chem. 257*, 12092–12100.

Hangarter, R. P., & Good, N. E. (1982) *Biochim. Biophys. Acta 681*, 397–404.

Hansen, U. P., Gradmann, D., Sanders, D., & Slayman, C. L. (1981) *J. Membr. Biol. 63*, 165–190.

Hill, T. L. (1977) *Free Energy Transduction in Biology*, Academic Press, New York.

Junge, W. (1970) *Eur. J. Biochem. 14*, 582–592.

Karlish, S. J. D., & Stein, W. D. (1982) *J. Physiol. (London) 328*, 295–316.

Kedem, O., & Caplan, S. R. (1965) *Trans. Faraday Soc. 61*, 1897–1911.

Kishimoto, U., Kami-ike, N., Takeuchi, Y., & Ohkawa, T. (1984) *J. Membr. Biol. 80*, 175–183.

Krishnamoorthy, G., & Hinkle, P. C. (1984) *Biochemistry 23*, 1640–1645.

Laidler, K. J. (1958) *The Chemical Kinetics of Enzyme Action*, Clarendon Press, Oxford.

Lang, M. A., Caplan, S. R., & Essig, A. (1977a) *Biochim. Biophys. Acta 464*, 571–582.

Lang, M. A., Caplan, S. R., & Essig, A. (1977b) *J. Membr. Biol. 31*, 19–29.

Lanyi, J. K., & Silverman, M. P. (1979) *J. Biol. Chem. 254*, 4750–4755.

Läuger, P. (1979) *Biochim. Biophys. Acta 552*, 143–161.

Lemasters, J. J., & Billica, W. H. (1981) *J. Biol. Chem. 256*, 12949–12957.

Lemasters, J. J., Grunwald, R., & Emaus, R. K. (1984) *J. Biol. Chem. 259*, 3058–3063.

Maloney, P. C. (1982) *Curr. Top. Membr. Transp. 16*, 175–193.

Maloney, P. C., & Schattschneider, S. (1980) *FEBS Lett. 110*, 337–340.

McCarthy, J. E. G., & Ferguson, S. J. (1983) *Eur. J. Biochem. 132*, 425–431.

Mills, J. D., & Mitchell, P. (1984) *Biochim. Biophys. Acta 764*, 93–104.

Mitchell, P. (1966) *Chemiosmotic Coupling in Oxidative and Photosynthetic Phosphorylation*, Glynn Research Ltd., Bodmin, U.K.

Nicholls, D. G., & Bernson, V. S. M. (1977) *Eur. J. Biochem. 75*, 601–612.

O'Neal, C. C., & Boyer, P. D. (1984) *J. Biol. Chem. 259*, 5761–5767.

Padan, E., & Rottenberg, H. (1973) *Eur. J. Biochem. 40*, 431–437.

Pietrobon, D., Azzone, G. F., & Walz, D. (1981) *Eur. J. Biochem. 117*, 389–394.

Pietrobon, D., Zoratti, M., Azzone, G. F., Stucki, J. W., & Walz, D. (1982) *Eur. J. Biochem. 127*, 483–494.

Pietrobon, D., Zoratti, M., & Azzone, G. F. (1983) *Biochim. Biophys. Acta 723*, 317–321.

Power, J., Cross, R. L., & Harris, D. A. (1983) *Biochim. Biophys. Acta 724*, 128–141.

Rothschild, K. J., Ellias, S. A., Essig, A., & Stanley, H. E. (1980) *Biophys. J. 30*, 209–230.

Rottenberg, H. (1973) *Biophys. J. 13*, 503–511.

Rottenberg, H. (1979) *Biochim. Biophys. Acta 549*, 225–253.

Rottenberg, H., & Gutman, M. (1977) *Biochemistry 16*, 3220–3227.

Schwab, W. G. W., & Komor, E. (1978) *FEBS Lett. 87*, 157–160.

Serpersu, E. H., & Tsong, T. Y. (1984) *J. Biol. Chem. 259*, 7155–7162.

Soumarmon, A., Rangachari, P. K., & Lewin, N. J. N. (1984) *J. Biol. Chem. 259*, 11861–11867.

Stucki, J. W. (1980a) *Eur. J. Biochem. 109*, 257–267.

Stucki, J. W. (1980b) *Eur. J. Biochem. 109*, 269–283.

Stucki, J. W., Compiani, M., & Caplan, S. R. (1983) *Biophys. Chem. 18*, 101-109.
Tanford, C. (1982) *Proc. Natl. Acad. Sci. U.S.A. 79*, 6161-6165.
Tuena de Gomez Puyou, M., Muller, U., Dreyfus, G., Ayala, G., & Gomez Puyou, A. (1983) *J. Biol. Chem. 258*, 13680-13684.
van Dam, K., Westerhoff, H. V., Krab, K., van der Meer, R., & Arents, J. C. (1980) *Biochim. Biophys. Acta 591*, 240-250.
van den Berg, G. B., Colen, A. M., Wanders, R. J. A., Westerhoff, H. V., & van Dam, K. (1982) *EBEC Reports 2*, 627-628.
van der Meer, R., Westerhoff, H. V., & van Dam, K. (1980) *Biochim. Biophys. Acta 591*, 488-493.
Wanders, R. J. A., Groen, A. K., van den Berg, G. B., Westerhoff, H. V., & Tager, J. M. (1982) *EBEC Reports 2*, 563-564.
Westerhoff, H. V. (1983) *Mosaic Non-Equilibrium Thermodynamics and (the Control of) Biological Free-Energy Transduction*, Ph.D. Thesis, University of Amsterdam, Amsterdam, The Netherlands.
Westerhoff, H. V., & Dancshâzy, Zs. (1984) *Trends Biochem. Sci. 9*, 112-117.
Wikström, M., Krab, K., & Saraste, M. (1981) *Cytochrome Oxidase: A Synthesis*, Academic Press, London.
Zoratti, M., Pietrobon, D., & Azzone, G. F. (1982) *Eur. J. Biochem. 126*, 443-451.
Zoratti, M., Favaron, M., Pietrobon, D., & Azzone, G. F. (1984) *EBEC Reports 3A*, 283-284.

Slow Transacylation of Peptidyladenosine Allows Analysis of the 2′/3′-Isomer Specificity of Peptidyltransferase†

Mutsuo Taiji, Shigeyuki Yokoyama,* and Tatsuo Miyazawa
Department of Biophysics and Biochemistry, Faculty of Science, University of Tokyo, Hongo, Bunkyo-ku, Tokyo 113, Japan
Received February 25, 1985

ABSTRACT: 2′-*O*-(*N*-acetyl-L-phenylalanyl-L-phenylalanyl)adenosine and 3′-*O*-(*N*-acetyl-L-phenylalanyl-L-phenylalanyl)adenosine (Ac-Phe-Phe-Ado) were chemically synthesized, and these two isomers were clearly separated from each other by high-performance liquid chromatography (HPLC) on an ODS column. By this HPLC method, the abundance ratio of the 2′-isomer and 3′-isomer in equilibrium in aqueous solution at pH 7.0 and 0 °C was found to be 0.30:0.70, and the equilibration rate was determined as 0.59 ± 0.04 min^{-1}. Thus, the rate of transacylation between the 2′-isomer and 3′-isomer of peptidyl-tRNA was found to be much slower than that for the two isomers of aminoacyl-tRNA. The HPLC method was used for isomer analysis of the product of the *Escherichia coli* ribosomal peptidyltransferase reaction. By the use of an *isomerizable* analogue, 2′(3′)-*O*-L-phenylalanyladenosine (Phe-Ado), as the acceptor of the *N*-acetyl-L-[^{3}H]phenylalanine (Ac-[^{3}H]Phe) group in the Ac-[^{3}H]Phe-tRNA^{Phe}·poly(U)·70S ribosome system, the reaction product was found exclusively to be the 3′-isomer of Ac-[^{3}H]Phe-Phe-Ado. Thus, the slow transacylation of peptidyladenosine allows the analysis of the 2′/3′-isomer specificity of peptidyltransferase.

In the process of protein biosynthesis, the CCA-terminal adenosine residue of a tRNA species is aminoacylated, by the cognate aminoacyl-tRNA synthetase, to form 2′-O-aminoacylated isomer (2′-isomer)[1] or 3′-O-aminoacylated isomer (3′-isomer). The 2′-isomer and 3′-isomer of an aminoacyladenosine moiety are shown in Figure 1a. The conversion between the 2′-isomer and 3′-isomer of aminoacyl-tRNA (transacylation) has long been believed to be as fast as 4 × 10^3 s^{-1}, with reference to the transacylation rate as estimated for formyladenosine in aqueous solution (Griffin et al., 1966). If the transacylation rate was as fast as estimated previously, it should be impractical to determine experimentally which isomer of aminoacyl-tRNA is required in individual steps of the protein biosynthesis process. Therefore, the 2′/3′-isomer specificities for aminoacyl-tRNA and peptidyl-tRNA have been analyzed by the use of nonisomerizable tRNA analogues, including those terminating in 2′-deoxyadenosine (2′-deoxy-Ado-tRNA) and in 3′-deoxyadenosine (3′-deoxy-Ado-tRNA) (Hecht, 1979; Sprinzl & Wagner, 1979; Wagner et al., 1982; Wagner & Sprinzl, 1983). Thus, Sprinzl and co-workers have concluded that the transacylation between the 2′-isomer and 3′-isomer is inevitably involved in the polypeptide chain elongation cycle (Sprinzl & Wagner, 1979; Wagner et al., 1982).

Actually, however, by the NMR saturation transfer method, we have succeeded in the experimental determination of the transacylation rates of aminoacyladenosines (Figure 1a) as faithful models for the CCA-terminal moiety of aminoacyl-tRNA species (Taiji et al., 1981). Surprisingly, in aqueous solution at pH 7.3 and 37 °C (intracellular environment), the transacylation rates are found to be as slow as 3-11 s^{-1} for the 2′ → 3′ transacylation and 1-4 s^{-1} for the 3′ → 2′ transacylation (Taiji et al., 1983). These transacylation rates are

† This work was supported in part by a Grant-in-Aid for Scientific Research (58780146) from the Ministry of Education, Science and Culture of Japan and by a grant from Takeda Science Foundation (Osaka, Japan).

[1] Abbreviations: Ac-Phe, *N*-acetyl-L-phenylalanine; Ac-Phe-Phe-Ado, 2′(3′)-*O*-(*N*-acetyl-L-phenylalanyl-L-phenylalanyl)adenosine; Ac-Phe-tRNA^{Phe}, *N*-acetyl-L-phenylalanyl-tRNA^{Phe}; Ado, adenosine; Bes, 2-[bis-(2-hydroxyethyl)amino]ethanesulfonic acid; 2′-deoxy-Ado-tRNA, tRNA terminating in 2′-deoxyadenosine; 3′-deoxy-Ado-tRNA, tRNA terminating in 3′-deoxyadenosine; HONB, *N*-hydroxy-5-norbornene-2,3-dicarboximide; HPLC, high-performance liquid chromatography; 2′-isomer, 2′-O-aminoacylated isomer; 3′-isomer, 3′-O-aminoacylated isomer; Phe-Ado, 2′(3′)-*O*-L-phenylalanyladenosine; Tris-HCl, tris(hydroxymethyl)aminomethane hydrochloride.

0006-2960/85/0424-5776$01.50/0